

Comparative Studies of Lensing Methods

Thomas P. Kling, Ezra T. Newman, and Alejandro Perez

University of Pittsburgh, Pittsburgh, PA, USA

(December 2, 2024)

Abstract

Predictions of the standard thin lens approximation and a new iterative approach to gravitational lensing are compared with an “exact” approach in simple test cases involving one or two lenses. We show that the thin lens and iterative approaches are remarkably accurate in predicting time delays, source positions and image magnifications for a single monopole lens. However, observationally significant errors were found when the thin lens method was applied to lensing configurations with two lenses. In these cases, the iterative method remained accurate beyond observational limits.

I. INTRODUCTION

In this paper, three different approaches to gravitational lensing are compared in test cases with one or two lenses. The three approaches include a recently introduced exact approach [1], which we will take as representing correct values in our comparisons, the thin lens approximation commonly used in lensing, and a new iterative technique whose zeroth iterate is given by the thin lens approximation [2]. An outline of these three methods will be given in Section II.

A recent paper by Frittelli, Kling, and Newman [3] discusses lensing in a Schwarzschild geometry and compares the exact approach with the standard thin lens approximation, a second order thin lens approximation, and a strong-field version of the thin lens approximation introduced by Virbhadra and Ellis [4]. In Schwarzschild spacetimes, it was found that the first and second order thin lens approximations fail dramatically when the light rays encounter strong gravitational fields. However, the strong field version of Virbhadra and Ellis, which is a hybrid lensing approach using some exact and some thin lens ideas, performed remarkably well in predicting the observation angle of a given source for a given observer and lens, even when the light ray circles the lens many times. In addition, it was found that the errors in the time delays predicted by the thin lens approximation compared with the values predicted by the exact method were small for cases resembling current observational scenarios, but, as the impact parameter was reduced, the error introduced by using the thin lens approximation became appreciable.

Here we are interested in studying the accuracy of the thin lens and iterative approaches to gravitational lensing in more detail. Specifically, we wish to address two questions:

1. Are the intrinsic errors introduced by using the thin lens approximation of comparable size to the observational errors present today or in the near future?
2. Are the corrections for lens structure, given in terms of higher multipole moments or some mass distribution function, utilized by the thin lens method, comparable to the inherent errors in the thin lens approximation?

With each of these questions, we are also interested in seeing if the iterative approach provides a significant improvement in accuracy. We will not examine the accuracy of other approximate techniques in the literature [5,6].

At this point, we do not wish to imply that the work presented here should be taken as a serious attempt at modeling real lens systems. Our intention is to show that there are reasonable domains where the corrections to the thin lens approximation are comparable in size to the observational errors today and also to the changes produced in predictions from lens models based on the thin lens approximation when structures are added.

To address these issues, several test cases involving one or two lenses will be examined. Three different lens configurations will be compared:

- i. a single spherically symmetric lens,
- ii. two identical lenses spatially collinear with the observer in two different lens planes,
- iii. two identical lenses located in a single lens plane.

For each of these scenarios, we will consider several comparisons:

1. the source location predicted by each method given the same lens configuration, observer, and observation angle,
2. the time delays between two rays predicted by each method given the same lens configuration, observer, and (two) observation angles.
3. the magnification (relative to an unlensed ray) predicted by each method given the same lens configuration, observer, and observation angle.

Section III will be devoted to these comparisons. The issue of the accuracy of the thin lens approximation was raised in Chapter 9 of [7], where a footnote reference is given to the work of P. Haines. One motivation of this paper is to extend the studies cited there.

In general, we find that, in the observational regime, the thin lens and iterative approaches are very accurate when applied to lensing by a single monopole lens. However, when two lenses are placed in the same lens plane so that the lens has “structure,” the error in the thin lens method can become comparable in size to observational errors in certain distance ranges between the two lenses. For lensing by single monopole lenses in multiple lens planes, the thin lens method is inaccurate when the distance between the two lens planes is small compared to the distance between either plane and the observer but large compared to the distance of closest approach either lens. In both of these situations, the iterative method remains quite accurate.

II. LENSING APPROACHES

In this section, we give brief outlines of the thin lens, exact and iterative approaches to lensing. For convenience, we will set $G = c = 1$ in our equations, although, in our final comparisons we will return to physical units (meters, days). Our convention for the signature of the metric is $(+, -, -, -)$.

A. The thin lens approximation

The thin lens approximation is the standard approach to gravitational lensing used by astrophysicists. In this subsection, we will only outline its basic premises and indicate several particular assumptions which we will use in our comparisons in Section III. Very thorough and pedagogical presentations of the thin lens methodology and its applications can be found in the excellent book by Falco, Schneider and Ehlers [7] and a paper by Blandford and Narayan [8].

In the standard approach, the lens is treated as a weak perturbation of a background spacetime. For convenience, two kinds of spatial planes are introduced: a source plane, where potential sources lie, and lens planes containing lensing bodies.

Kinematically possible paths from an observer at the point O to a source at a point S in the source plane will be connected, piecewise smooth segments of geodesics in the background space. For example, if there is one lens plane, the trajectories from S to O will pass through the lens plane at the image point I, as shown in Fig. 1. The paths from S to I and from I to O are geodesics in the background metric with no influence from the lens. The only influence of the lens on the trajectory occurs at I, where the direction of the geodesic is instantaneously changed by an amount determined by a bending angle. The thin lens bending angle is a function of a mass distribution in the lens plane and the point I.

For a single, spherically symmetric lens with mass m , the bending angle, α , is given by

$$\alpha = \frac{4m}{|\vec{\xi}_o|}, \quad (1)$$

where $|\vec{\xi}_o|$ is the magnitude of the two dimensional vector in the lens plane locating the point I relative to the lens. This bending angle is the first order bending angle obtained in a Schwarzschild spacetime between the future and past asymptotes of a null ray connecting points at future and past null infinity. If there are many monopole lenses in the plane located at $\vec{\xi}_i$ with masses m_i , the bending angle is given by adding the first order contributions of the individual bending angles

$$\vec{\alpha} = \sum_{i=1}^n \frac{4m_i}{|\vec{\xi}_i - \vec{\xi}_o|^2} (\vec{\xi}_i - \vec{\xi}_o). \quad (2)$$

The vectorial bending angle, $\vec{\alpha}$, gives the two dimensional bending angle in the lens plane. Note that if there is more than one lens plane, the bending angle in each plane will be influenced only by the lenses in that plane. Continuous mass distributions are obtained by replacing the summation in Eq. (2) by an integral and integrating a mass distribution over the entire lens plane.

If the mass distribution is known, the entire thin lens trajectory can be codified into a lens equation. If $\vec{\theta}$ is an angle locating the image of a lensed source and $\vec{\beta}$ is the “observation angle in the absence of the lens” given in Fig. 1, the lens equation for one lens plane is

$$\vec{\beta} = \vec{\theta} - \frac{D_{ls}}{D_s} \vec{\alpha}. \quad (3)$$

An important quantity in lensing is the time which elapses between the emission of the light ray and its interception by the observer, or the time of arrival. Although we will not use the ideas here, the time of arrival serves as a Fermat potential from which one can derive the lens equation, Eq. (3). Individual arrival times are not an observable, but the time delay between two images of the same source is an important quantity which has been measured in several lens systems [9]. (The time delay can be used, with other observations, to determine the Hubble constant.)

Returning to the general case with many lenses in many lens planes, the time of arrival in the thin lens approximation is given by

$$t = \int_{SIO} (1 + 2U(l)) dl, \quad (4)$$

where $U(l)$ is the Newtonian potential of the mass distribution, and the integral is taken along the thin lens trajectory parameterized by an Euclidean length l from the source at S to through the image point at I to the observer at O . For a collection of masses, the Newtonian potential is

$$U(l) = \sum_{i=1}^n \frac{m_i}{|\vec{r}(l) - \vec{r}_i|}. \quad (5)$$

In Eq. (5), \vec{r}_i is a three dimensional vector locating lenses relative to some origin while $\vec{r}(l)$ is the vector locating points along the thin lens path parameterized by a Euclidean length along the trajectory. Time delays are given by the difference in two such times.

In this paper, we will choose Minkowski spacetime as our background. We do not anticipate that there would be significant differences in our results using Robertson-Walker or on-average Robertson-Walker metrics as the background spacetime, although we have not examined this question.

B. Exact lensing

The key difference between the exact approach to gravitational lensing and the thin lens approximation is that, in the exact approach, the lens is fully incorporated into a metric satisfying Einstein’s equations. In this way, no background / lens splitting is introduced and no quantities defined in the thin lens method as “in the absence of a lens” have meaning.

Lensing information in the exact approach is obtained by integrating the null geodesic equations of the metric [1]. A particular parametric form of the null geodesic equations are defined to be the lens and time of arrival equations. It can be shown that in a Schwarzschild spacetime, the lens and time of arrival equations can be expressed parametrically in local, timelike coordinates as

$$t = T(R, \theta_o, \phi_o, x_o^a) \quad (6)$$

$$x^i = X^i(R, \theta_o, \phi_o, x_o^a) \quad (7)$$

where (t, x^i) label points on the past light cone of an observer located at x_o^a [3]. The two “angular parameters,” (θ_o, ϕ_o) , represent the direction on an observer’s celestial sphere where the image is observed, and R can be taken as a physical distance to the source such as the angular-diameter distance. Equation (6) is defined to be the exact time of arrival equation while Eqs. (7) are the exact lens equations.

The first comparison which we will consider in this paper is lensing in Schwarzschild spacetimes. The time of arrival and lens equations for a Schwarzschild spacetime can be found in closed form by integrating the null geodesics of the Schwarzschild metric using its symmetries [10]; however, in the current work, we will not use these closed form expressions for the lens and time of arrival equations. Instead, we will solve the null geodesic equations by forming a Hamiltonian,

$$H(x^c, p_c) = g^{ab}(x^c) p_a p_b, \quad (8)$$

and numerically solving Hamilton’s equations of motion. Null geodesics are obtained when the initial conditions, (x_o^a, p_a^o) , satisfy

$$H(x_o^c, p_c^o) = 0. \quad (9)$$

We will refer to the numerical integrations of the geodesic equations as the “exact” approach or method.

By performing a coordinate transformation,

$$\begin{aligned} t &= t \\ r &= \sqrt{x^2 + y^2 + z^2} \\ \theta &= \arctan \frac{z}{\sqrt{x^2 + y^2}} \\ \phi &= \arctan \frac{y}{x}, \end{aligned} \quad (10)$$

we can write the Schwarzschild metric as

$$g^{ab}(x^a) = \begin{pmatrix} 1/(1 - \frac{2m}{r}) & 0 & 0 & 0 \\ 0 & -1 + \frac{2mx^2}{r^3} & \frac{2mxy}{r^3} & \frac{2mxz}{r^3} \\ 0 & \frac{2mxy}{r^3} & -1 + \frac{2my^2}{r^3} & \frac{2myz}{r^3} \\ 0 & \frac{2mxz}{r^3} & \frac{2myz}{r^3} & -1 + \frac{2mz^2}{r^3} \end{pmatrix}. \quad (11)$$

These coordinates are useful for comparing the “exact” method to the thin lens and iterative methods. Hence, we solve Hamilton’s equations of motion in a (t, x, y, z) coordinate system which is adapted to comparisons with the thin lens and iterative approaches.

We are also interested in comparing the three lensing methodologies in situations with more than one lens. Since there are no exact solutions to Einstein’s equations to meet these lensing configurations, one can not apply the exact methodology. For these cases, we will consider approximate metrics whose null geodesics are solved using Hamilton’s equations of motion. In these cases, we will call the numerical solution to Hamilton’s equations for null geodesics of the approximate metric the “exact” time of arrival and lens equations.

C. Iterative approach

The iterative approach seeks to improve upon the thin lens approximation and can be applied to any approximate solution to Einstein's equations which is close to a spacetime in which the exact method can be employed. In this paper, we will focus on the first iterate only, although higher iterates can be obtained. Details on the iterative approach, including equations for the first iterate method applied to a Schwarzschild spacetime, can be found in [2].

The general method is to assume that the spacetime of interest, (M, g^{ab}) , is close to some spacetime, (M, g_o^{ab}) , where the geodesic equations can be solved exactly. This means that we can write the metric g^{ab} as

$$g^{ab}(x^c) = g_o^{ab}(x^c) + h^{ab}(x^c)$$

where the components of $h^{ab}(x^c)$ are small.

One begins the iterative method by forming the Hamiltonians in both spacetimes,

$$H(x^c, p_c) = g^{ab}(x^c) p_a p_b = g_o^{ab}(x^c) p_a p_b + h^{ab}(x^c) p_a p_b \quad (12)$$

$$H_o(x^c, p_c) = g_o^{ab}(x^c) p_a p_b, \quad (13)$$

and solving the Hamilton-Jacobi equation in (M, g_o^{ab}) :

$$g_o^{ab}(x^c) \frac{\partial F}{\partial x^a} \frac{\partial F}{\partial x^b} + \frac{\partial F}{\partial \lambda} = 0. \quad (14)$$

In spacetimes in which the geodesic equations can be solved, one can always find a solution to the Hamilton-Jacobi equation of the form

$$F = F_o(x^c, P_c, \lambda) \quad (15)$$

in which λ is a parameter and P_c are four constants. This function can be taken as the generating function for a parameter dependent, canonical transformation,

$$(x^c, p_c) \rightarrow (X^c, P_c). \quad (16)$$

If (M, g_o^{ab}) is taken to be Minkowski spacetime, (M, η^{ab}) , the solution to the Hamilton-Jacobi equation, Eq. (14) is

$$F_o(x^c, P_c, \lambda) = x^a P_a - \eta^{ab} P_a P_b \lambda, \quad (17)$$

and the canonical transformation to the coordinates (X^c, P_c) is given by

$$x^a = X^a - 2\eta^{ab} P_b \lambda \quad (18)$$

$$p_a = P_a. \quad (19)$$

When this canonical transformation is applied to the Hamiltonian in (M, g^{ab}) , the transformed Hamiltonian takes a particularly simple form

$$H(x^c, p_c) \rightarrow H'(X^c P_c, \lambda) = h^{ab}(X^c, P_c, \lambda) P_a P_b. \quad (20)$$

Hamilton's equations for geodesics in the (X^a, P_a) coordinates are

$$\begin{aligned} \dot{X}^a &= 2h^{ab}(X^c, P_c, \lambda) P_b + \left(\frac{\partial h^{bc}}{\partial P_a}(X^c, P_c, \lambda) \right) P_b P_c \equiv \Xi^a(X^a, P_a, \lambda) \\ \dot{P}_a &= - \left(\frac{\partial h^{bc}}{\partial X^a}(X^c, P_c, \lambda) \right) P_b P_c \equiv \Pi_a(X^a, P_a, \lambda). \end{aligned} \quad (21)$$

No approximations have been made to obtain these equations.

We wish to solve Hamilton's equations, Eqs. (21), by iteration. For the zeroth iterate, we must specify eight functions

$$\begin{aligned} X_0^a &= X_0^a(X_o^a, P_a^o, \lambda) \\ P_a^0 &= P_a^0(X_o^a, P_a^o, \lambda), \end{aligned} \quad (22)$$

and substitute these functions of λ and initial conditions, $x_o^a = X_o^a$ and $p_a^o = P_a^o$, into the right hand side of Hamilton's equations, Eqs. (21). (Care should be taken to choose the eight functions serving as the zeroth iterate close to the true description of the path of the null geodesic.) The first iterate is obtained by direct integration on λ :

$$\begin{aligned} X_1^a(X_o^a, P_a^o, \lambda) &= X_o^a + \int_0^\lambda d\lambda' \Xi^a(X_o^a, P_a^0, \lambda') \\ P_a^1(X_o^a, P_a^o, \lambda) &= P_a^o + \int_0^\lambda d\lambda' \Pi_a(X_o^a, P_a^0, \lambda'). \end{aligned} \quad (23)$$

Likewise, the n th iterate is obtained by placing $(X_{n-1}^a(X_o^a, P_a^o, \lambda), P_a^{n-1}(X_o^a, P_a^o, \lambda))$ into the right hand side of Eqs. (21) and integrating up.

The n th iterate solution to Hamilton's equations in the original spacetime coordinates, (x^a, p_a) , is obtained by placing $(X_n^a(X_o^a, P_a^o, \lambda), P_a^n(X_o^a, P_a^o, \lambda))$ into the canonical transformation, Eq. (18) and (19):

$$x_n^a(X_o^a, P_a^o, \lambda) = X_n^a(X_o^a, P_a^o, \lambda) - 2\eta^{ab} P_b^n(X_o^a, P_a^o, \lambda) \lambda \quad (24)$$

$$p_a(X_o^a, P_a^o, \lambda) = P_a^n(X_o^a, P_a^o, \lambda). \quad (25)$$

In these equations, $(X_o^a = x_o^a, P_a^o = p_a^o)$ are the initial values for the approximate geodesic. When these initial conditions satisfy the null condition on the Hamiltonian in Eq. (12),

$$H(X_o^a = x_o^a, P_a^o = p_a^o, \lambda = 0) = g^{00}(x_o^a) (p_0^o)^2 + g^{ij}(x_o^a) p_i^o p_j^o = 0, \quad (26)$$

the geodesics are approximately null. Solving Eq. (26) for p_0^o yields

$$p_0^o = \sqrt{\frac{-g^{ij}(x_o^a) p_i^o p_j^o}{g^{00}(x_o^a)}}. \quad (27)$$

We will make use of this expression below.

To make a deeper connection with lensing, we will take the thin lens path as the zeroth iterate. As an example, we show the explicit zeroth iterate for the case of one spherical lens in one lens plane.

For one spherically symmetric lens, the thin lens path would be given by

$$\begin{aligned} x_{(1)}^i &= x_o^i - 2\delta^{ij} p_j^o \lambda & 0 < \lambda < \lambda_1 \\ x_{(2)}^i &= x_{(1max)}^i - 2\delta^{ij} \tilde{p}_j^o \lambda & 0 < \lambda, \end{aligned} \quad (28)$$

where $x_{(1)}^i$ describes the first leg (to the lens plane), $x_{(2)}^i$ describes the second leg away from the lens plane and (x_o^i, p_i^o) are constant initial conditions. If we locate the observer at $-|z_o|$ on the $-\hat{z}$ axis, we can use spherical symmetry to consider geodesics in the \hat{x} - \hat{z} plane. Then the $z = 0$ plane is the lens plane, and the value of λ_1 is

$$\lambda_1 = \frac{|z_o|}{2 p_z^o}. \quad (29)$$

We also have that

$$x_{(1max)}^i = x_o^i - \frac{\delta^{ij} p_j^o |z_o|}{p_z^o}. \quad (30)$$

Using the bending angle, $\alpha = 2m/|x_{(1max)}^i|$, the \tilde{p}_j^o will be determined up to scaling through the Minkowski spatial inner product between p_j^o and \tilde{p}_j^o :

$$\cos \alpha = \frac{(p_x^o)(\tilde{p}_x^o) + (p_z^o)(\tilde{p}_z^o)}{|p_i^o| |\tilde{p}_i^o|}. \quad (31)$$

If we multiply and divide the right hand side in Eq. (31) by $1/(p_z^o \tilde{p}_z^o)$ and define

$$p = \frac{p_x^o}{p_z^o} \quad \text{and} \quad \tilde{p} = \frac{\tilde{p}_x^o}{\tilde{p}_z^o},$$

Eq. (31) is equivalent to a quadratic equation for \tilde{p} in terms of p and α . Solving this equation gives

$$\tilde{p} = \frac{p \pm \cos \alpha \sin \alpha \sqrt{(1 + p^2)^2}}{\cos^2 \alpha - p^2 \sin^2 \alpha}. \quad (32)$$

We now return to the issue of the value of $p_0^o = P_0^o$. In this paper, the iterative method will only be applied to stationary spacetimes. Hence, the timelike coordinate, t , will not appear in the original Hamiltonian, Eq. (12), and T , the canonically transformed variable, will not appear in the transformed Hamiltonian, Eq. (20). As T is cyclic, the time equation, (\dot{T}) , will separate from the spatial equations. Moreover, because T does not appear in the Hamiltonian,

$$\dot{P}_0 = -\frac{\partial H'}{\partial T}$$

will be identically zero so that $P_0 = p_0$ is constant. The value of this constant must be chosen to make the trajectory null, as in Eq. (27). However, there is an inherent scaling

freedom of the null vector which permits us to define new four-momenta, $p_a^{'o}$ which are a constant multiple of the old one.

It is customary to fix the freedom in the scaling of the null vector by *defining* $p_0^{'o} = 1$. Then in the case of a single monopole lens, the equation

$$p_0^o \equiv 1 = \sqrt{\frac{-g^{ij}(x_o^a) p_i^o p_j^o}{g^{00}(x_o^a)}}, \quad (33)$$

gives an equation for the initial p_z^o in terms of the p_x^o and the initial point.

As we take the thin lens trajectory as the zeroth iterate, we will choose to set the value of p_0^o to one at the initial point (the observer, O) and again in each lens plane. In this way, $p_0^o = \tilde{p}_0^o = 1$, and the relative scaling of (p_x^o, p_z^o) and $(\tilde{p}_x^o, \tilde{p}_z^o)$ is uniquely determined using Eq. (33).

Summarizing, the spatial part of the zeroth iterate for a one lens system is given by the thin lens path, Eq. (28). The observer is located at the initial point x_o^a . For a given value of p_x^o , p_z^o is uniquely determined by the condition $p_0^o = 1$, from Eq. (33). The new $(\tilde{p}_x^o, \tilde{p}_z^o)$ are determined using the bending angle as in Eq. (32) and the condition $\tilde{p}_0^o = 1$.

So far, our discussion has only considered cases with axial symmetry and one lens plane. If there is more than one lens plane, the procedure we have described above is extended to each lens plane. If there is no axial symmetry, there will be a complementary equation to the bending angle relation, Eq. (31), which can be used to fix the three spatial components of the momenta in an analogous way to what we have presented here.

In the cases we will study, the time coordinate is cyclic and the time equation in the original phase space variables is simply the integral equation

$$t = t_o + \int 2 p_0^o (1 + 2 U(x^a(\lambda))) d\lambda, \quad (34)$$

where $U(r)$ is the Newtonian potential of the mass distribution. The integral is taken over the path as a function of the parameter λ . The first iterate time is obtained when the path inserted into Eq. (34) is the zeroth order, thin lens path, $x^a(\lambda) = x_o^a(\lambda)$. Hence the first iterate time is precisely the value obtained in the standard thin lens approximation. However, as we will find the first iterate trajectories, we can also find the second iterate time values by evaluating the integrand in Eq. (34) along the first iterate, $x^a(\lambda) = x_1^a(\lambda)$.

A conceptual problem arises in computing the iterative time of arrival if one uses the formula

$$t_n = t_o + 2 \int p_0 d\lambda (1 + U(x_{n-1}^a(\lambda))) \quad (35)$$

for the n th iterate time. In general, the parameter λ should be an affine parameter along a null geodesic. We note that if Hamilton's equations are solved exactly, fixing p_0^o as in Eq. (27) ensures that the value of the Hamiltonian will be zero at all points along the path and λ will be an affine parameter. However, in the iterative method, the geodesic equations are not solved exactly, and the value of the Hamiltonian will slowly drift away from zero. Hence, as λ grows, it fails to be an affine parameter along a null geodesic.

A way to force the Hamiltonian to be zero, and hence λ to be null affine parameter, is to allow p_0 to be a function along the trajectory given by

$$p_0 = p_0^n(\lambda) = \sqrt{\frac{-g^{ij}(x_n^a) p_i^n p_j^n}{g^{00}(x_n^a)}}, \quad (36)$$

where (x_n^a, p_a^n) are the n th iterate values. This proposal leads to a conflict between maintaining the null value of the Hamiltonian along the n th iterate trajectory

$$H(x_n^a, p_a^n, \lambda) = 0 \quad (37)$$

and Hamilton's equation,

$$\dot{p}_0 = 0. \quad (38)$$

Since we are dealing with static cases, a consistent proposed solution is to take p_0 as constant in the spatial Hamilton's equations, but allow p_0 to vary as in Eq. (36) when computing times. This solution disentangles the two competing problems given in Eq. (37) and Eq. (38) by obeying Hamilton's equations when integrating the spatial part of the geodesic and also obeying the null condition in computing the times (which is very sensitive to integrating over an affine parameter).

Hence, when comparing the iterative time delays to the “exact” and thin lens delays, we will consider the time of arrivals given by

$$t_2 = t_o + \int 2 p_0^1(\lambda)(1 + 2 U(r_1)) d\lambda. \quad (39)$$

We will show that this formula gives very accurate predictions for time delays in our comparisons.

III. COMPARISON OF LENSING APPROACHES

In this section we present the results obtained in the comparison of time delays, source location and image magnification predicted by the thin lens approximation and the iterative method for several different lens models. The comparisons are made with respect to the numerical integration of the exact geodesic equations of the spacetime metric defined by the given model. For the iterative method, we will be interested in the first iterate only.

There are four subsections in this section. In the first, we give details regarding the comparisons we will be discussing. We then group our comparisons in three sets. First, we consider lensing by a single spherical lens, or the Schwarzschild geometry. Next, we consider multiple lensing by single monopole lenses collinear with the observer in different lens planes. Finally, we consider lensing by two lenses in the same lens plane. In our plots, all angles are given in arc seconds and all times are given in days.

A. Notes about comparisons

We will be comparing the predictions of the thin lens, iterative and “exact” approaches to lensing for time delays, source locations and image magnification. In this subsection, we

give some details about how these comparisons are performed. We will refer to the spatial axis connecting the lens and observer as the optical axis.

First, we note that the exact solution to the geodesic equation produces an infinite number of images [3], but that the thin lens approximation predicts only two of these images for the case of a single lens (referred to as primary images). This feature is shared by the first iterate method, since it corresponds to the next step in the perturbative series whose zeroth order is given by thin lens approximation (the first iterate method should give sensible predictions as long as its trajectory remains close to the thin lens trajectory). However, it is not difficult to choose the two primary exact images corresponding to the thin lens and first iterate images because these primary images are widely separated (in angular location) from the secondary images which circle the lens one time.

Throughout our comparisons, we will refer to an observation angle, θ . This angle is computed by taking the inner product between the spatial part of the initial momentum vector, p_i^o , at the observer and the spatial vector pointing to the lens from the observer's location, x_o^o . Formally, this must be done using the spatial metric describing the model. However, as we will always be taking this inner product at a large distance from the lens, it is appropriate to take the observation angle, θ , as the ratio of the \hat{x} and \hat{z} components of the initial momentum:

$$\theta = \frac{p_x^o}{p_z^o}.$$

To compare the time delays predicted by the three methods, we must compute the two trajectories from each method, integrate the arrival time function along each trajectory, and subtract the two values we obtain. We begin by choosing two initial angles, (θ_1, θ_2) , one on each side of the lens. These angles are chosen such that trajectories with these initial conditions intersect at a reasonable distance beyond the last lens; usually, this distance is chosen as approximately the same as the distance between the observer and the first lens. For each path, we compute the time of arrival and subtract the two times to get a time delay. We will then hold one angle, θ_2 , fixed while varying θ_1 . This allows us to plot the time delay as a function of θ_1 for a fixed θ_2 .

In practice, finding the time delays is a very difficult calculation, as the arrival times for each trajectory will agree in roughly their first 12 digits (at our scales). The comparison between the methods is even more difficult, as the time delays from the three methods tend to agree to about four digits. Hence, to resolve a difference between the thin lens, iterative, and “exact” predictions for the time delays, we must know the arrival time to approximately 16 digits of accuracy.

To compute the source location, β , for a given observation angle, θ , we choose a value of θ and a final distance along the optical axis from the observer, D_s . If the optical axis is the \hat{z} axis and the observer is located at $z = -|z_0|$, we then place a plane at $z = D_s - |z_0|$ which will be the “source plane.” We then compute, for a given initial condition, θ , the interception point in the source plane, $\vec{\eta}$. The value of β is *defined* to be

$$\beta = \frac{|\vec{\eta}|}{D_s}. \quad (40)$$

We will use this definition for the source location in all three models. As θ is varied, we will obtain $\beta(\theta)$.

Magnifications are defined as $\frac{\partial\theta}{\partial\beta}$, or the inverse slope of the β versus θ graph. We will compute the magnifications from the data we obtain in our β - θ comparisons. Note that this magnification is not directly observable; we discuss it only because it plays a role in the literature. With some additional work, we could compute, for two given images, (θ_1, θ_2) , the relative magnification,

$$\mu_{12} = \frac{\left(\frac{\partial\theta}{\partial\beta}\right)_{\theta_2}}{\left(\frac{\partial\theta}{\partial\beta}\right)_{\theta_1}},$$

which is observable. We plan to return to this possible comparison in future work.

In the two lens models, the thin lens approximation predicts four images. Therefore, in the calculation of the time delays we can distinguish three qualitatively different situations. As it is illustrated in Fig. 2, there is a range for θ_1 and θ_2 for which the two rays cross the optical axis between the two lenses and then converge at the observer's position (range A), a range for which only one of the rays crosses the region between the lenses (range B), and, finally, a range in which none of the rays cross the axis until they meet at the observer's position (range C). When looking at magnifications and image positions, we can compare the three methods in two cases: 1) rays which do not cross between the two lenses and 2) rays which do cross the optical axis between the lenses.

B. One spherical lens

Here we discuss the comparisons between the first iterate, thin lens and “exact” predictions for various observables when there is one spherically symmetric lens. For the “exact” predictions, we consider the numerical integration of the geodesic equations of the exact Schwarzschild metric, as specified in Section II.B. As mentioned, Minkowski spacetime will be considered the background spacetime for the iterative and thin lens approaches.

For our comparisons, we will take a lens 7.5×10^{22} km away from the observer with a mass of $5 \times 10^{12} M_\odot$. If we were concerned with a cosmological model, a linear redshift to distance relation,

$$d = \frac{cz}{H_o},$$

with Hubble constant, $H_o = 60$ km/s Mpc, gives that 7.5×10^{22} km is approximately a redshift of $z \approx 0.5$. Hence, our one lens model represents lensing by a somewhat massive, distant galaxy.

In Fig. 3a we show the position of the source, β , as a function of the image position, θ , (see Fig. 1) calculated using the exact numerical integration of the geodesics equations. The range in θ has been chosen in agreement with observed image angles in systems with similar characteristics as the one represented by our model, and the value of D_s has been set equal to the observer-lens spacing. The absolute error in β between the exact numerical integration and the thin lens approximation and the first iterate method are shown in Fig. 3b. The discrepancies between the two methods are of about 10^{-5} arc sec. In Fig 4a, we show the “exact” magnification $M = \frac{\partial\theta}{\partial\beta}$ as a function of the image position θ . The relative error,

$$\Delta M_{tl,it} = \frac{M_{tl,it} - M_{ex}}{M_{ex}},$$

in the predicted magnification by the two approximate methods is shown in Fig 4b. The errors here are very small.

In the case of a single spherically symmetric lens, we were not able to resolve the difference in the time delay error between the thin lens and first iterate trajectories. Our calculations showed that this error was indeed quite small, and that for a lens with mass $5 \times 10^{12} M_{\odot}$ at 7.5×10^{22} km from the observer, the error in the thin lens and iterative methods was less than 0.2 days when the “exact” time delay was 400 days.

C. Two lenses in different lens planes

In this subsection, we will consider lensing by two identical lenses aligned with the observer with a mass of 5×10^{12} solar masses. Depending on the distance between the two lenses, D_{12} , the errors in the thin lens and iterative methods have different properties. When the masses are very far apart, both methods are reasonably accurate; however, if the two lenses are close together, possibly members of the same overall group, the thin lens method performs poorly. We will examine the case where the lenses are far apart first.

1) Large separation

In our first comparisons, we consider an observer 7.5×10^{22} km away from the first lens and set the distance between the two lenses equal to the distance between the observer and the first lens. Figure 5a shows the “exact” image location, β , as a function of observation angle, θ , when the light ray does not cross between two lenses and $D_s = 2.25 \times 10^{23}$ km, or three times the spacing between the first lens and observer. As before, the error in the thin lens and first iterate methods, shown in Fig. 5b, are small. At a fairly large observation angle, $4.3''$ from the optical axis, the error in the thin lens method is about 10^{-4} arc sec. The “exact” magnification and errors in the thin lens and iterative methods for this lens configuration are shown in Fig. 6.

For the same lensing configuration, the “exact” source location and the error in the thin lens and iterative methods when the light ray crosses the optical axis is shown in Fig. 7. In this case, the light ray passes much closer to the lens, and we see that the first iterate is slightly better than the thin lens in predicting the source location. The corresponding magnifications are plotted in Fig. 8.

When the two lenses are separated by the same distance as the observer-lens₁ distance, the time delays predicted by the thin lens and iterative method are very accurate. As in the one lens case, we were unable to resolve a difference in the time delays due to the high precision required in any of the three possible ray combinations from Fig. 2. Our calculations show that the error in the thin lens and first iterate methods was less than 0.1 days for a time delay around 500 days.

2) Small separation

Very interesting results were obtained when the distance between the two lenses was small. As an example, we will examine the case where the observer and two lenses lie along the same optical axis, the mass of each lens is $5 \times 10^{12} M_{\odot}$, the distance to the first lens from the observer is 7.5×10^{22} km meters and the distance between the two lenses is 7.5×10^{19} km. This second distance is slightly larger than the distance between our galaxy and Andromeda, so that our lensing configuration represents a pair of lenses at roughly the same redshift (around $z \approx .5$). Thus, we may think of this example as corresponding to direct lensing by two members of the same group. In this case, it makes sense to choose D_s as twice the distance to the first lens. $D_s = 1.5 \times 10^{23}$ km.

When the lenses are so close together, it does not make sense to consider rays crossing between the two lenses; to pass between the lenses, the observation angle must be less than $0.125''$. Because this observation angle does not look reasonable, we note only in passing that the time delays, magnifications, and source locations predicted by the thin lens method are in very poor agreement with the “exact” approach, while the iterative method represents a modest improvement.

Substantial errors do occur in the thin lens method for the case where the rays remain outside the two lenses. In Fig. 9, we show the “exact” source angle as a function of the observation angle and the error in the thin lens and first iterate approaches. We note that the error in the thin lens method is quite large, $\beta_{ex} - \beta_{tl} \approx 0.035''$. This error is large enough to be observed. The first iterate remains accurate in this region; the error in the first iterate method is less than $0.0002''$ for the range in θ shown.

A similar result is found in the magnifications, shown in Fig. 10. Here, we note that the thin lens method is about five times less accurate than the first iterate.

In Fig. 11a, we plot the “exact” time delay predicted by numerical integration of the geodesic equations of the metric. The fixed angle, θ_2 , was set to $2.475''$ and the range in θ_1 is shown. Figure 11b shows three error curves. The solid curve towards the lower part of the graph is the error in the first iterate method. The curve is not smooth due to numerical noise, but we can determine that at an “exact” time delay of 400 days, the iterative method, given by the integral in Eq. (39), is less than 0.15 days. The long dashed curve represents the error in the thin lens approximation; at 400 days, this error is a little over one day, which is close to the current level of observational accuracy.

Because the lenses are so close together, one may think that it is appropriate to treat them as a single lens located in the middle of the two with a total mass equal to the sum of the values of the two masses. When the thin lens approximation is applied to a single lens with the total mass of the system, the error in the time delay is larger at this separation. The dotted curve represents the error in the time delay predicted by the thin lens approximation when the lensing configuration is treated as one lens with the total mass located directly between the two lenses.

Essentially, the thin lens method fails in these cases because it is not a good approximation to ignore the effect of lenses outside of the lens plane when computing the bending angle. The iterative method does not suffer from this drawback because, although the zeroth iterate is chosen as the thin lens path, at all points along the trajectory both lenses influence the change in direction in a continuous manner. We will discuss this issue further in the conclusion.

The error in the thin lens time delays, source angle and magnification have maximum values for a separation distance between the two lenses. To show this, we compare time delays for the three methods where we fix the two observation angles to $(\theta_r = 2.475'', \theta_l = 2.7392'')$ and vary the distance between the two lenses, whose masses are each $5 \times 10^{12} M_\odot$. In Fig. 12a, we plot the “exact” time delay as a function of the distance between the two lenses in units of 10^{18} kilometers. Figure 12b shows that there is a maximum error in the time delay predicted by the thin lens method at roughly 2×10^{18} km for our model. At this lens separation, the error in the thin lens method is very large (10%), but the error in the first iterate predictions, which are not shown, are minimal.

The distance at which the thin lens method is most at error in our comparison is 10 times larger than the radius of our galaxy, and therefore, is not astrophysically significant. However, as we see in Figs. 11 and 9, a sizeable error persists as the distance is increased to galactic spacings, two orders of magnitude larger than this spacing for the maximum error. The effect is negligible and the error in the thin lens approximation can not be distinguished from numerical noise above a distance between the lenses of 10^{21} km.

D. Two lenses in the same lens plane

As a final comparison, we consider two lenses in the same lens plane. Here we will take each lens to have a mass of $2.5 \times 10^{12} M_\odot$ and will set the lens plane 7.5×10^{22} km away from the observer. This case resembles the one lens system in that the distances are the same but the mass has been split. We choose a separation of 7.5×10^{16} km between the lenses. For our comparisons of β and magnification, we will take D_s to be twice the spacing between the lens and observer.

Figure 13 shows the “exact” plot of source angle, β , versus observation angle, θ , and the error in β for the thin lens and iterative method. The “exact” magnifications and relative errors are shown in Fig. 14. As in the case of the two lenses close together, there is a significant difference in the accuracy of the thin lens and iterative methods. The “exact” time delay and errors are plotted in Fig. 15. The error curves for time delays become somewhat jumpy at large θ values due to numerical noise. When the exact time delay is 400 days, the first iterate error is about 0.025 days while the thin lens error is around 0.65 days. We find that this error grows as the separation between the two lenses increases.

IV. DISCUSSION

We have performed a careful examination of the accuracy of two lensing approximations, the thin lens and iterative methods, in scenarios with one and two monopole lenses. In general, we find that source locations, time delays and magnifications computed using the first iterate are more accurate than those computed with the thin lens.

Both methods are accurate beyond the current level of observational error when the deflector was a single spherical lens or two lenses separated by a large distance. The cases we studied in this paper tended to involve rather massive lenses. Since the thin lens and iterative methods generally become more accurate as the mass is decreased holding the distances the same, we feel that it is likely that lensing by objects resembling well separated

monopole lenses with smaller masses will be well described by both the thin lens and iterative methods.

It was found that the thin lens approximation was not accurate in predicting time delays, magnifications or source locations in the cases we studied with two lens which are close together. For our choices of distance scales and masses, the error in the thin lens method was often of the same order of magnitude as the current limits of observation. In these cases, the iterative method did provide a significant improvement over the thin lens approximation.

The failure of the thin lens method in cases where multiple lenses are close raises three interesting questions for lensing. First, are there lensing scenarios where multiple members of a group strongly lens a source? In this case, the assumption that each galaxy can be considered separately in its own lens plane may not be justified. An alternative version of this question is whether lens structure which extends along the line of sight to the lens can be compressed into a two-dimensional lens plane. It seems that when there is a three dimensional mass distribution, collapsing the distribution into a single lens plane may lead to a poor approximation.

Second, our calculation of two lenses in one lens plane suggests that the inclusion of lens structure can significantly influence the performance of the thin lens approximation. A question that requires further study is whether two dimensional continuous mass distributions of the type used in lens modeling lead to inaccuracies in the thin lens approximation which might corrupt current efforts at using lensing to predict various cosmological parameters.

As a third question, we are interested in how our results apply to microlensing by binary systems. It is estimated that nearly ten percent of microlensing events will be microlensing by binary systems. At various points in time, the rotating bodies will resemble either two lenses in different lens planes or two lenses in the same lens plane, which are similar to our case studies. One key difference is that, in general, the mass to distance ratio in microlensing will be smaller than the ratios we have studied. This will tend to reduce the error we detected in the thin lens method. On the other hand, as the source moves across the sky, the light rays from the source come very close to the binary lens. We found a rather large error in the thin lens method when the distance of closest approach was on the same order of magnitude as the separation between the lenses. Hence, we do not know what the accuracy of the thin lens method will be when applied to microlensing by binaries. We will study this issue in future work.

The current observational abilities allow resolution of angles up to milli arc sec and errors of about one day for time delays. Likewise, efforts to fit observational data to lens models often fail at similar scales even when many free parameters are introduced. In this paper, we showed that the intrinsic errors of the thin lens approximation can approach these levels in cases where two lenses are close together, either in one lens plane or in two. This suggests that the thin lens method should be applied very carefully or modified in these cases. The iterative method provides one such improvement over the thin lens and seems to be reasonably accurate in all the cases we have studied.

Acknowledgments

The authors would like to thank David Turnshek, Al Janis, Simonetta Frittelli and Jurgen Ehlers for their helpful advice and suggestions. Alejandro Perez would like to thank FUNDACION YPF. This work was supported under grants Phy 97-22049 and Phy 92-05109.

REFERENCES

- [1] S. Frittelli and E. T. Newman, Phys. Rev. D **59**, 124001, (1999).
- [2] T. P. Kling, E. T. Newman and A. Perez, gr-qc/9908082, to be published in Phys. Rev. D, (2000).
- [3] S. Frittelli, T. P. Kling, and E. T. Newman, gr-qc/001037, to be published in Phys. Rev. D, (2000).
- [4] K. S. Virbhadra and G. F. R. Ellis, astro-ph/9904193, to be published in Phys. Rev. D, (2000).
- [5] T. Pyne and M. Birkinshaw, ApJ, **415**, 459, (1993).
- [6] T. Pyne and M. Birkinshaw, ApJ, **458**, 46, (1996).
- [7] P. Schneider, J. Ehlers, and E. E. Falco, *Gravitational Lenses*, (Springer-Verlag, New York, Berlin, Heidelberg, 1992).
- [8] R. Blandford and R. Narayan, ApJ **310**, 568-582, (1986).
- [9] Harvard-Smithsonian Center for Astrophysics website for lensing, <http://cfa-www.harvard.edu/castles/>.
- [10] T. P. Kling and E. T. Newman, Phys. Rev D **59**, 124002, (1999).

FIGURES

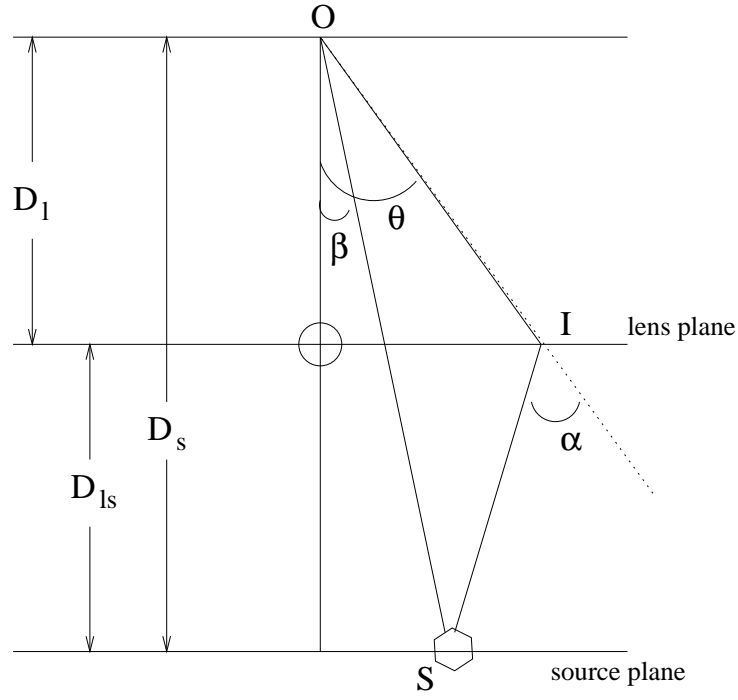


FIG. 1. Schematic illustration of the thin lens method for a single lens.

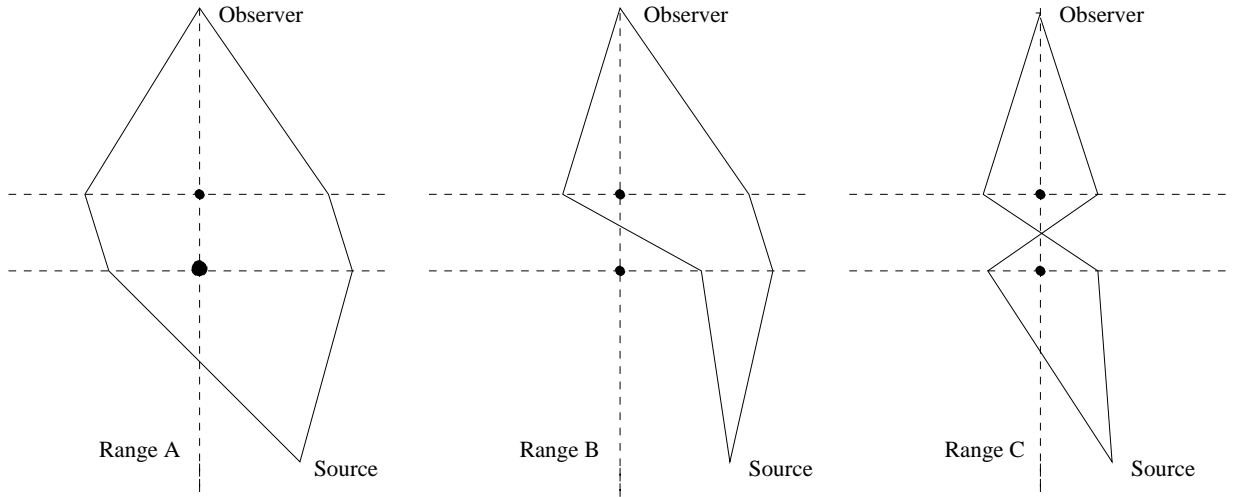


FIG. 2. Schematic illustration of the different lensing scenarios for the two lens model.

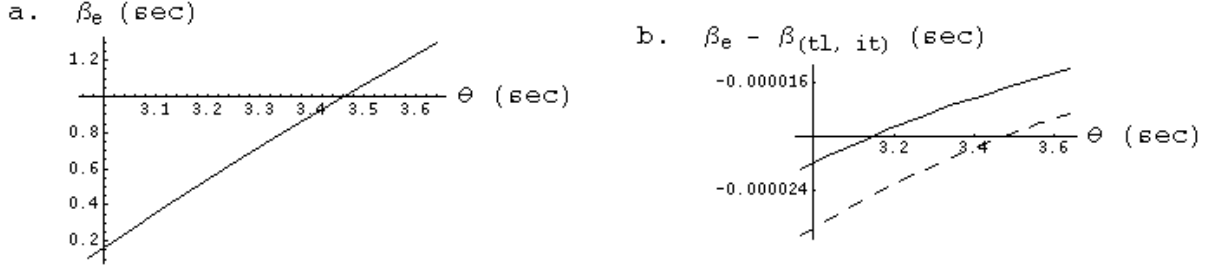


FIG. 3. a. Exact angular position of the source, β , as a function of the image position, θ , in arc sec. b. Error in the angular position of the source as a function of θ . The first iterate error ($\beta_{ex} - \beta_{it}$) and the thin lens approximation error ($\beta_{ex} - \beta_{tl}$) are represented by a smooth line and a dashed line respectively, in arc sec.

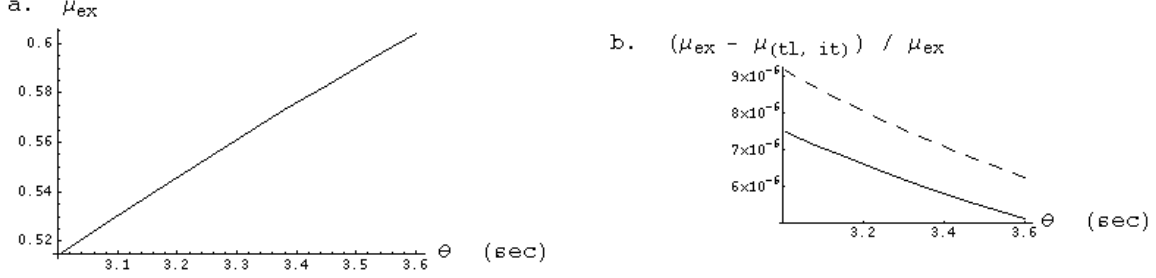


FIG. 4. a. Exact magnification as a function of θ . b. Relative error in the magnifications predicted by the first iterate and thin lens are represented by smooth and dashed lines, respectively, as a function of θ .

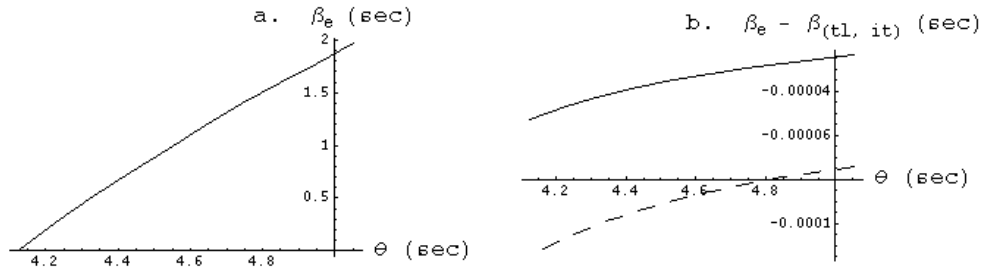


FIG. 5. a. Exact angular position of the source, β , as a function of the image position for two lenses separated by a distance equal to the separation of the first lens and observer when the light ray does not cross the optical axis. b. Error in the angular position of the source predicted by the first iterate and thin lens, represented by smooth and dashed lines respectively.

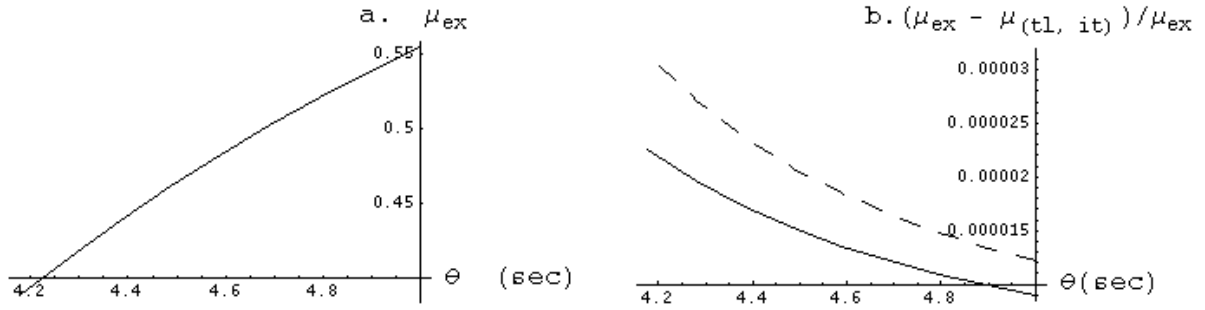


FIG. 6. a. Exact magnification as a function of θ for two lenses separated by a distance equal to the separation of the first lens and observer when the light ray does not cross the optical axis. b. Relative error in the magnifications predicted by the first iterate and thin lens, represented by smooth and dashed lines respectively.

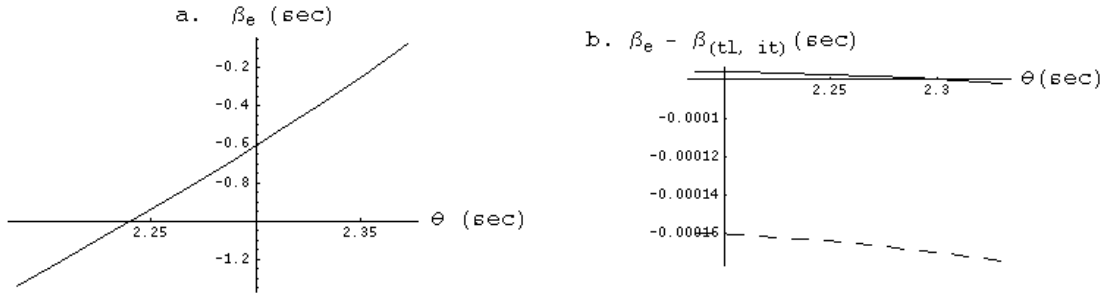


FIG. 7. a. Exact angular position of the source, β , as a function of the image position for two lenses separated by a distance equal to the separation of the first lens and observer when the light ray crosses the optical axis. b. Error in the angular position of the source predicted by the first iterate and thin lens, represented by smooth and dashed lines respectively.

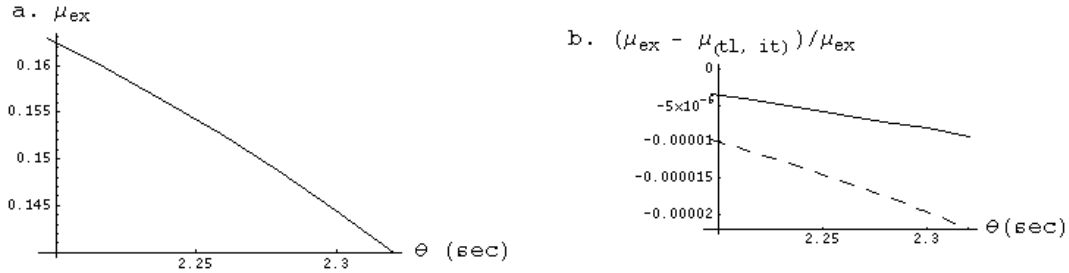


FIG. 8. a. Exact magnification as a function of θ for two lenses separated by a distance equal to the separation of the first lens and observer when the light ray crosses the optical axis. b. Relative error in the magnifications predicted by the first iterate and thin lens, represented by smooth and dashed lines respectively.

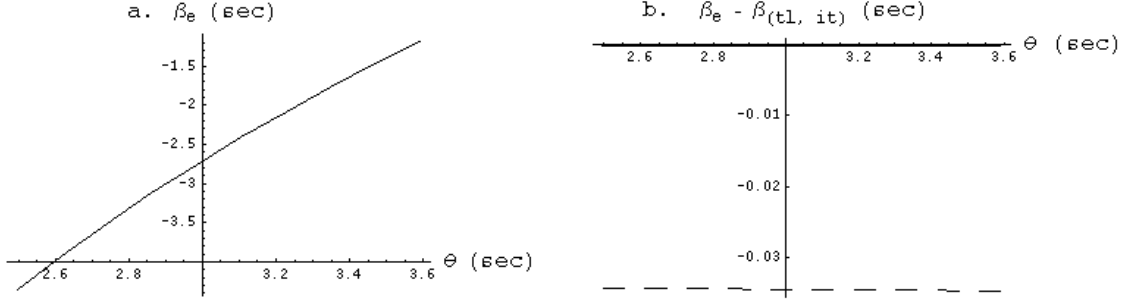


FIG. 9. a. Exact angular position of the source, β , as a function of the image position for two lenses separated by a small distance compared with the separation of the first lens and observer. b. Error in the angular position of the source predicted by the first iterate and thin lens, represented by smooth and dashed lines respectively.

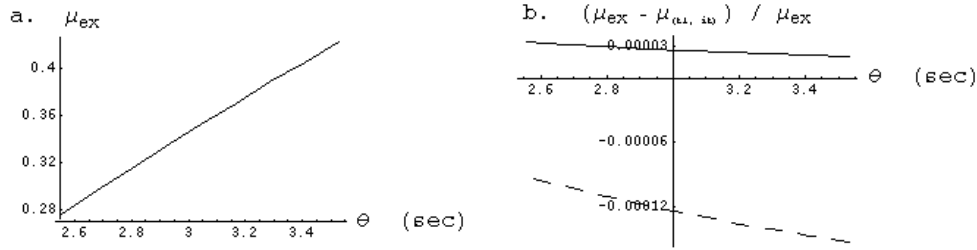


FIG. 10. a. Exact magnification as a function of θ for two lenses separated by a small distance compared with the separation of the first lens and observer. b. Relative error in the magnifications predicted by the first iterate and thin lens, represented by smooth and dashed lines respectively.

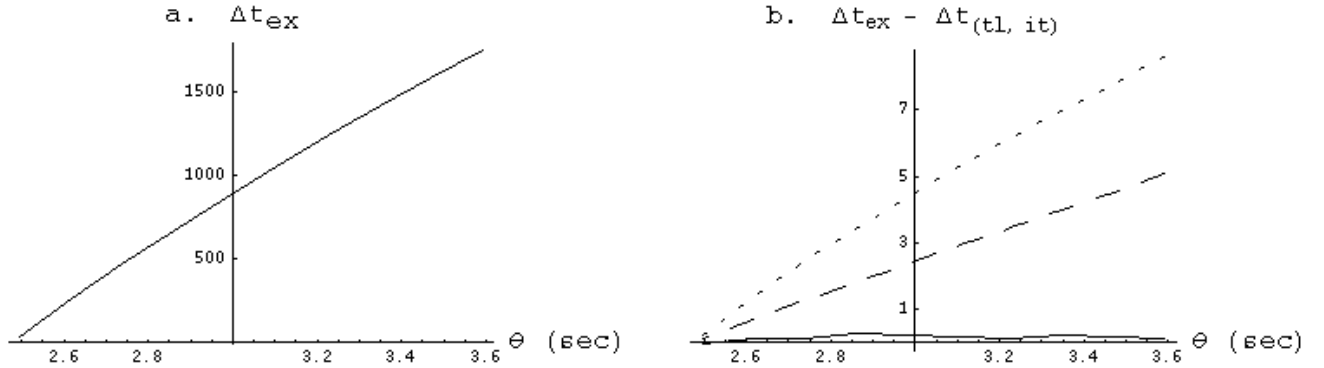


FIG. 11. a. Exact time delay as a function of θ_1 for two lenses separated by a small distance compared with the separation of the first lens and observer when $\theta_2 = 2.475''$. b. Error in the time delays predicted by the first iterate and thin lens methods, represented by smooth and dashed lines. The error in the time delay predicted by a second thin lens approximation where the two lenses are grouped together is represented by the dotted line.

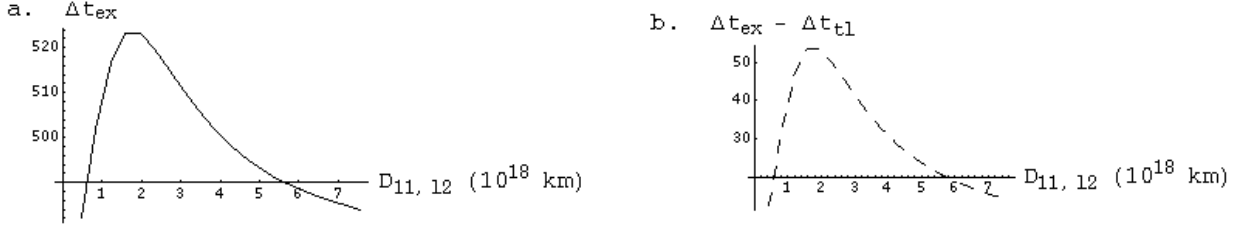


FIG. 12. a. Exact time delay as a function of the distance between the two lenses for fixed observation angles. b. Error in the time delays predicted by the thin lens methods.

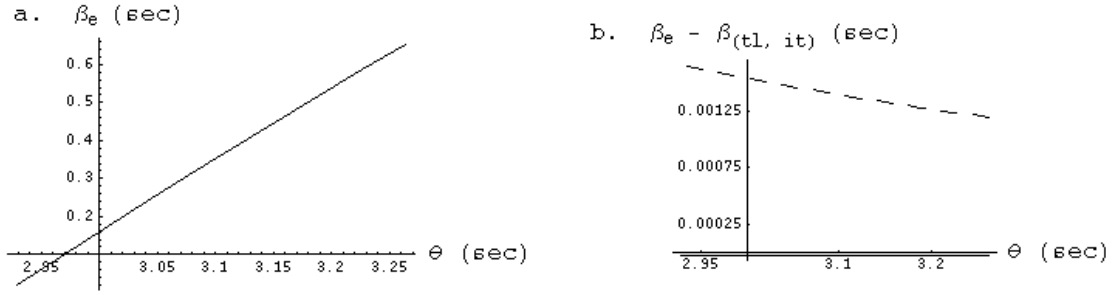


FIG. 13. a. Exact angular position of the source β as a function of the image position for two lenses in the same lens plane. b. Error in the angular position of the source predicted by the first iterate and thin lens, represented by smooth and dashed lines respectively.

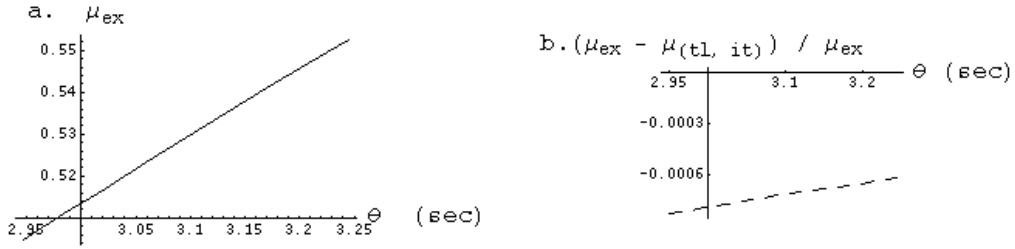


FIG. 14. a. Exact magnification as a function of θ for two lenses in the same lens plane. b. Relative error in the magnifications predicted by the first iterate and thin lens, represented by smooth and dashed lines respectively.

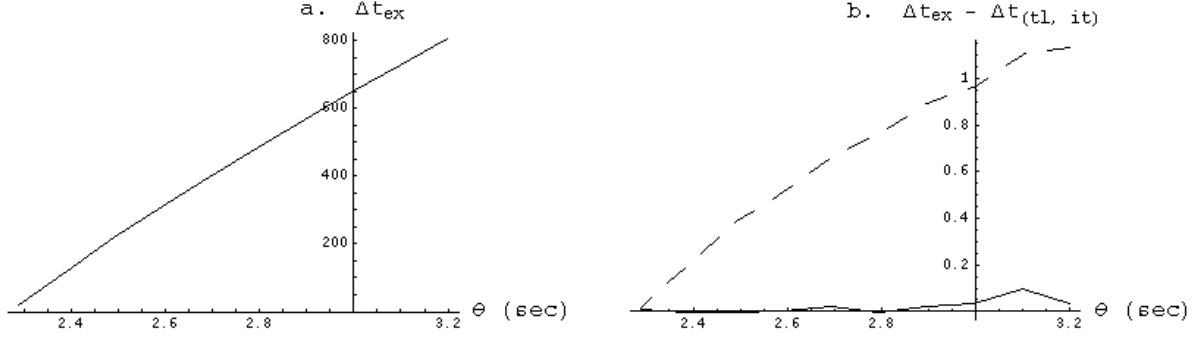


FIG. 15. a. Exact time delay as a function of θ_1 for two lenses in the same lens plane when $\theta_2 = 2.269''$. b. Error in the time delays predicted by the first iterate and thin lens methods, represented by smooth and dashed lines respectively.